Assessment of Physiologic Intracranial Calcification in Healthy Adults Using ^{18}F-NaF PET/CT

Abdullah Al-Zaghal[1], Siavash Mehdizadeh Seraj[1], Thomas J. Werner[1], Oke Gerke[2], Poul F. Høilund-Carlsen[2,3], and Abass Alavi[1]

[1]Department of Radiology, Hospital of University of Pennsylvania, Philadelphia, Pennsylvania; [2]Department of Nuclear Medicine, Odense University Hospital, Odense, Denmark; and [3]Department of Clinical Research, University of Southern Denmark, Odense, Denmark

The aim of this research study was to determine the role of ^{18}F-sodium fluoride (^{18}F-NaF) PET/CT imaging in the assessment of physiologic molecular calcification in the intracranial structures. We also examined the association of ^{18}F-NaF accumulation with age as well as Hounsfield unit (HU) in certain anatomic sites that are known to calcify with normal aging. **Methods:** A total of 78 healthy subjects from the Cardiovascular Molecular Calcification Assessed by ^{18}F-NaF PET/CT (CAMONA) clinical trial (38 women and 40 men) were included in this retrospective study. The mean age was 45.28 ± 14.15 y (age range, 21–75 y). SUV_{mean} was used to measure ^{18}F-NaF accumulation in the choroid plexus and epithalamus (pineal gland and habenula). Maximum HU was also measured for each region of interest. Correlation analysis was conducted to assess the association between parameters. **Results:** Mean SUV_{mean} was 0.42 ± 0.26 in the right choroid plexus, 0.39 ± 25 in the left choroid plexus, and 0.23 ± 0.08 in the epithalamus. Significant positive correlations were present between ^{18}F-NaF uptake and age in the right choroid plexus ($r = 0.61$, $P < 0.0001$), left choroid plexus ($r = 0.63$, $P < 0.0001$), and epithalamus ($r = 0.36$, $P = 0.001$). ^{18}F-NaF uptake significantly correlated with HU in the right choroid plexus ($r = 0.52$, $P < 0.0001$), left choroid plexus ($r = 0.57$, $P < 0.0001$), and epithalamus ($r = 0.25$, $P = 0.03$). **Conclusion:** ^{18}F-NaF could be used in the assessment of physiologic calcification in several intracranial structures. We report significant associations between ^{18}F-NaF uptake and aging as well as HU in the calcified choroid plexus and epithalamus. Our findings further support the growing interest to use ^{18}F-NaF for detecting extraosseous, molecular calcification, and this powerful probe has potential applications in the evaluation of various age-related, neurodegenerative brain processes.

Key Words: NaF; choroid plexus; pineal gland; brain calcification; PET

J Nucl Med 2019; 60:267–271
DOI: 10.2967/jnumed.118.213678

Sodium fluoride labeled with ^{18}F (^{18}F-NaF) was first used as a molecular imaging probe in 1962 by Blau et al. (*1*) and was approved by the U.S Food and Drug Administration in 1972 for routine assessment of osseous disorders including metastasis from various malignancies. ^{18}F-labeled NaF gained a great deal of popularity as an excellent bone-seeking agent due to its high skeletal uptake and rapid blood clearance from the circulation after its intravenous administration. However, due to lack of appropriate imaging instruments (PET), efforts were made to synthesize compounds that could be used with conventional nuclear medicine techniques. Therefore, routine use of ^{18}F-NaF declined since conventional γ-cameras were unable to detect the high-energy positron annihilation after ^{18}F decay. The introduction of modern PET scanners and the increased availability of ^{18}F-NaF have resulted in a renewed interest in this tracer. Its sensitivity in detecting benign and malignant osseous disorders is significantly higher than that of ^{99m}Tc-labeled phosphates (*2–4*).

Extraosseous accumulation of ^{18}F-NaF as a marker of soft-tissue calcification has been reported in many settings (*5,6*). ^{18}F-NaF uptake in the arterial wall of arteries such as the aorta and carotid and coronary arteries indicates an active calcifying atherosclerotic plaque (*7–9*). ^{18}F-NaF is also taken up in the extraosseous microscopic calcification, dystrophic calcification, and calcified metastatic lesions (*10–13*).

Intracranial calcification is a common neuroimaging finding in otherwise asymptomatic, normal individuals or in patients with a wide range of underlying maladies such as neurologic, metabolic, infectious, hemorrhagic, neoplastic, or other disorders (*14*). Choroid plexus calcification is very common finding, usually in the atrial portions of the lateral ventricles. Pineal region calcification is known to be present histologically from fetal life to adulthood. Idiopathic intracranial calcification is defined as the deposition of calcium within brain parenchyma in the absence of neurologic deficits or an apparent underlying pathologic cause (*15*). During the human life span, the choroid plexus, pineal gland, and habenula tend to accumulate physiologic calcifications.

The purpose of this study was to determine the use of ^{18}F-NaF PET in the detection and characterization of active calcification in intracranial structures. We also investigated the possible association between ^{18}F-NaF uptake and age as well as Hounsfield unit (HU) at the sites selected for this research project.

MATERIALS AND METHODS

^{18}F-NaF PET/CT scans used in this retrospective study are part of the Cardiovascular Molecular Calcification Assessed by ^{18}F-NaF PET/CT (CAMONA) protocol. CAMONA is a prospective trial and was approved by the Danish national committee on biomedical research ethics, registered at ClinicalTrials.gov (NCT01724749), and conducted from 2012 to 2016 in accordance with the Declaration of Helsinki. Details of the CAMONA study were previously published by Blomberg et al. (*16*).

Received Apr. 25, 2018; revision accepted Jun. 18, 2018.
For correspondence or reprints contact: Abass Alavi, Department of Radiology, Hospital of University of Pennsylvania, 3400 Spruce St, Philadelphia, PA 19104.
E-mail: abass.alavi@uphs.upenn.edu
Published online Jul. 12, 2018.

Subject Selection

The CAMONA study included 89 healthy volunteers who were recruited from the general population by local advertisement or from the blood bank of Odense University Hospital, Denmark. Negative history of cardiovascular disease, oncologic disease, chronic inflammatory disease, autoimmune disease, immunodeficiency syndromes, alcohol abuse, illicit drug use, or any prescription medication were inclusion criteria for healthy volunteers. Active smokers and pregnant women were excluded. Adults were preselected by sex and age to ensure a balanced inclusion of men and women aged 20–29, 30–39, 40–49, 50–59, and 60 y or older.

The Framingham risk score was used to evaluate the modifiable cardiovascular risk factors, and only subjects with a score below the upper limits of the recommended levels were included: systolic blood pressure below 160 mm Hg and a diastolic blood pressure below 100 mm Hg, total serum cholesterol below 6.2 mmol/L, and glycated hemoglobin (HbA1c) below 48 mmol/L (*17*). Further detailed description of the healthy subjects of the CAMONA study were previously published by Blomberg et al. (*18*).

In the current study, 6 subjects were excluded as their scans were not available within our laboratory database. Another 5 subjects were excluded because of motion artifact that degraded image quality and prevented optimal images analysis. A total of 78 healthy subjects, 38 women and 40 men, were included; mean age was 45.28 ± 14.15 y (age range, 21–75 y) (Table 1). The Danish national committee on biomedical research ethics approved this study, and all subjects signed a written informed consent form.

Study Design

Study participants were evaluated by blood pressure measurements, blood chemistry testing, Framingham risk score, and ^{18}F-NaF PET/CT imaging. Information regarding smoking habits, family history of cardiovascular diseases, and prescription medication were collected through questionnaires. Three blood pressure measurements were done for each patient, with an interval of 30 min while the patient rested supine. The average of last 2 systolic and diastolic measurements were recorded. Blood chemistry tests included fasting total cholesterol, serum low-density lipoprotein cholesterol, high-density lipoprotein cholesterol, fasting serum glucose, HbA1c, serum creatinine, and the Modification Diet and Renal Disease–estimated glomerular filtration rate. SCORE percentage was calculated for each subject based on sex, age, total serum cholesterol, serum high-density lipoprotein cholesterol, systolic blood pressure, and smoking status.

^{18}F-NaF PET/CT scans were obtained according to the previously published methodology by Blomberg et al. (*19*). In summary, ^{18}F-NaF PET/CT imaging was performed on integrated PET/CT scanners (Discovery 690, VCT, RX, and STE; GE Healthcare) with comparable spatial resolutions. PET images were obtained 90 min after the intravenous administration of 2.2 MBq of ^{18}F-NaF/kg of body weight. The acquisition time per bed position was 2.5 min. Total body PET images were acquired in 3-dimensional mode and reconstructed into coronal, transverse, and sagittal slices by an iterative reconstruction algorithm (VUE Point; GE Healthcare). Corrections were applied for attenuation, scatter, random coincidences, and scanner dead time. For

TABLE 1
Subject Demographics

Characteristic	Sex		*P*	Total (*n* = 78)
	Female (*n* = 38)	Male (*n* = 40)		
Age (y)	45.28 ± 14.56	45.27 ± 13.93	0.99	45.28 ± 14.15
BMI (kg/m^2)	25.30 ± 3.12	27.57 ± 4.31	<0.01	26.46 ± 3.92
BP (mm Hg)				
Systolic	124.75 ± 17.03	133.88 ± 16.91	0.02	129.43 ± 17.47
Diastolic	74.55 ± 10.39	78.61 ± 9.64	0.07	76.63 ± 10.15
Creatinine (mmol/L)	71.44 ± 9.97	87.72 ± 9.91	<0.01	79.79 ± 12.83
MDRD-eGFR (mL/min/1.73m^2)	79.52 ± 13.66	83.72 ± 12.63	0.16	81.67 ± 13.23
Serum blood sugar (mmol/L)	5.36 ± 0.50	5.66 ± 0.43	<0.01	5.51 ± 0.48
HbA1c (mmol/L)	33.05 ± 3.54	34.55 ± 4.56	0.10	33.82 ± 4.14
Fibrinogen (mmol/L)	9.20 ± 1.50	9.04 ± 1.37	0.63	9.12 ± 1.42
WBC (10^9/L)	5.79 ± 1.56	6.22 ± 2.14	0.28	5.99 ± 1.88
Triglyceride (mmol/L)	0.84 ± 0.30	1.26 ± 0.85	<0.01	1.06 ± 0.67
Cholesterol (mmol/L)				
Total	4.99 ± 0.86	4.86 ± 0.87	0.50	4.92 ± 0.86
LDL	2.98 ± 0.79	3.11 ± 0.79	0.50	3.05 ± 79
HDL	1.69 ± 0.46	1.20 ± 0.29	<0.01	1.44 ± 0.45
PET/CT systems				
GE Discovery STE	23	16		39
GE Discovery RX	8	17		25
GE Discovery 690/710	7	7		14
GE Discover VCT	0	0		0

Values are mean ± SD.

BP = blood pressure; BMI = body mass index; MDRD-eGFR = glomerular filtration rate estimated by the Modification of Diet and Renal Disease formula; WBC = white blood cells; LDL = low-density lipoprotein; HDL = high-density lipoprotein.

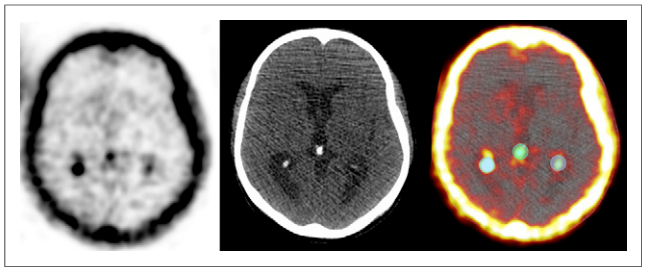

FIGURE 1. Axial PET, CT, and fused PET/CT brain images of a 59-y-old man illustrating ROIs set over calcified epithalamus and right and left choroid plexus. Mean ^{18}F-NaF uptake and maximum HU were measured for each ROI.

attenuation correction and anatomic orientation, low-dose CT imaging (140 kV, 30–110 mA, noise index 25, 0.8 s per rotation, slice thickness 3.75 mm) was performed. Total body PET images were acquired in 3-dimensional mode and reconstructed into coronal, transverse, and sagittal planes by an iterative reconstruction algorithm (VUE Point; GE Healthcare).

Image Analysis

Osirix MD, version 9.0 (DICOM viewer and image-analysis program; Pixmeo SARL) was used for the analysis of fused PET/CT images. Three fixed-size spheric regions of interest (ROIs) (volume = 1.5 cm^3, diameter = 1.42 cm) were drawn to encompass the calcified choroid plexus in the inferior horn of the lateral ventricle in each cerebral hemisphere and the epithalamus (including both the pineal gland and the habenula) (Fig. 1). SUV_{mean} and maximum HU were measured for each ROI.

Statistical Analysis

Correlation analysis by means of Pearson correlation coefficients and scatterplots was performed to investigate the relation of age with ^{18}F-NaF uptake and maximum HU values. The association between ^{18}F-NaF uptake and maximum HU was also investigated by correlation analysis. Exploratory multivariable linear regression was applied for all endpoints using all available demographic data (Supplemental Table 1; supplemental materials are available at http://jnm.snmjournals.org). Because of the limited sample size, the number of explanatory variables was reduced by application of variance inflation factor analysis first and backward variable selection (with $p_{stay} = 0.7$) thereafter, but age and sex were maintained irrespectively of their P values. A 2-tailed P value below 0.05 was regarded as statistically significant. Statistical analysis was conducted using Stata/MP 15.0 (StataCorp.).

RESULTS

SUV_{mean} was 0.42 ± 0.26 in the right choroid plexus, 0.39 ± 0.25 in the left choroid plexus, and 0.23 ± 0.08 in the epithalamus. The average of maximum HU was 148 ± 66.01 in the right choroid plexus, 141 ± 61.31 in the left choroid plexus, and 235 ± 130.69 in the epithalamus.

Significant positive correlations were present between ^{18}F-NaF uptake and age in the right choroid plexus ($r = 0.61$, $P < 0.0001$), left choroid plexus ($r = 0.63$, $P < 0.0001$), and epithalamus ($r = 0.36$, $P = 0.001$). HU values also had a positive correlation with aging in both the right ($r = 0.43$, $P = 0.0001$) and the left ($r = 0.40$, $P = 0.0003$) choroid plexus, but not in the epithalamus ($r = 0.19$, $P = 0.09$) (Fig. 2). Exploratory multivariable linear regression supported the statistically significant influence of age on ^{18}F-NaF uptake and HU values after adjustment for demographic variables (Supplemental Table 1).

Significant positive correlations were observed between ^{18}F-NaF uptake and HU in the right choroid plexus ($r = 0.52$, $P < 0.0001$), left choroid plexus ($r = 0.57$, $P < 0.0001$), and epithalamus ($r = 0.25$, $P = 0.03$) (Fig. 3).

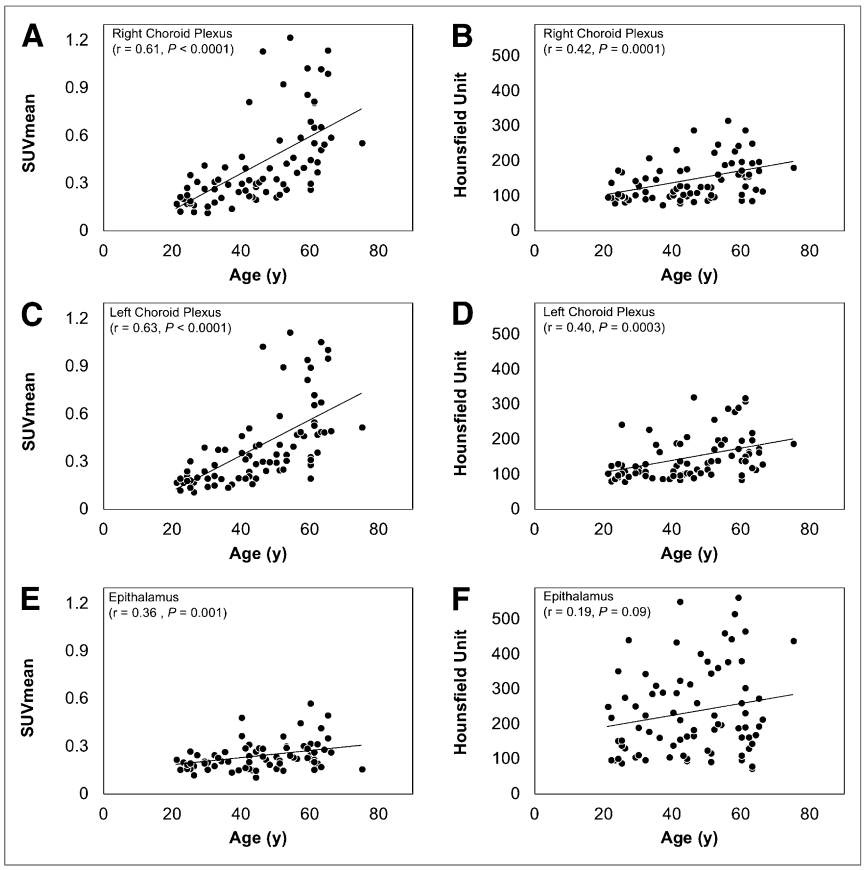

FIGURE 2. Correlation of ^{18}F-NaF uptake (A, C, E) and maximum HU (B, D, F) in choroid plexus and epithalamus with age. r = Pearson correlation coefficient.

DISCUSSION

Idiopathic intracranial calcification is thought to be related to normal physiologic aging and neurodegenerative processes (*20*). It is most commonly found in the choroid plexus, pineal gland, habenula, and dura matter. It is present in 50%–70% of adults above the age of 30 y, and its incidence increases with age (*21,22*), but it is not uncommon to encounter these finding in young adolescents (*23,24*).

Hydroxyl-apatite ($Ca_{10}[PO_4]_6[OH]_2$) is a major component of calcified intracranial lesions (*25,26*). The ^{18}F-fluorine ion of NaF exchanges with hydroxyl ions (OH^-) on the surface of the hydroxyapatite matrix to

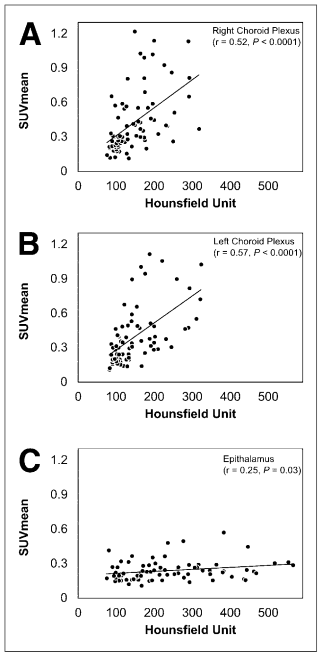

FIGURE 3. Correlations of ^{18}F-NaF uptake with HU values in right choroid plexus (A), left choroid plexus (B), and epithalamiums (C). r = Pearson correlation coefficient.

form fluoro-apatite (*27*). The rate of ^{18}F-NaF accumulation depends on the number of binding sites on the surface of hydroxyl-apatite available to react with ^{18}F (*28*). Any anabolic or catabolic process that alters calcium metabolism affects the hydroxyl-apatite surface area, and thus, increases the degree of availability of binding sites, consequently resulting in higher ^{18}F-NaF uptake (*29–31*).

Our results showed that ^{18}F-NaF PET could detect and semiquantify calcium metabolism and its turnover in calcified choroid plexus and epithalamus. We also found significant positive associations between aging and ^{18}F-NaF accumulation as well as HU values in the choroid plexus and epithalamus. ^{18}F-NaF accumulation in the regions selected for this study had a significant positive correlation with HU values.

Kwak et al. retrospectively studied 2,877 cranial CT scans and noted a strong association between the calcification of choroid plexus and pineal gland with normal aging (*32,33*). Whitehead et al. examined head CT scans of 500 subjects in their first decade of life and reported a correlation between choroid plexus and pineal gland calcification with age (*34*).

In the population examined, calcification in the epithalamus had higher maximum HU values than those seen in the choroid plexus on CT images. However, the choroid plexus had higher ^{18}F-NaF uptake on PET. This may indicate that calcium deposits in the pineal gland were more mature and less metabolically active than the calcification of the choroid plexus. This consolidates the role of PET as a functional imaging modality that reflects the metabolic activity of the investigated organ in contrast to other structural imaging modalities. Pathologic studies suggested that the architecture of pineal gland calcifications does not change with age (*35*).

Imaging studies are routinely used in the evaluation of brain calcifications and its associated disorders. Nonenhanced CT scanning is the most commonly used modality to image brain calcification; calcium deposits have a distinct hyperdense appearance on CT (*36,37*). Calcifications have variable signal intensity on T1-weighted and T2-weighted images. However, iron and calcium deposition in the basal ganglia both have a hypointense signal on T2-weighted images (*38*), making conventional MRI less reliable than CT in detecting calcifications (*39*). Susceptibility-weighted imaging has improved the ability of MRI in detecting brain calcification (*40*). The sensitivity of ultrasound for detecting intracranial calcification is highly comparable to that of CT in early childhood, but it is only feasible to perform in newborns before the closure of the fontanelles which occurs by the 18th month of age (*41,42*). Plain radiography is not a reliable modality to detect intracranial calcification, but extensive calcifications could be seen on radiographs as opaque lesions similar to that in the pineal gland or the falx.

Our study was limited by the imaging protocol; images were acquired 90 min after administration of ^{18}F-NaF instead of the routine 60 min-protocol; however, these scans originate as stated from the CAMONA project, which deals with molecular arterial calcification, whereas the Society of Nuclear Medicine and Molecular Imaging guideline is for ^{18}F-NaF PET/CT bone scans. Molecular imaging with PET to detect intracranial calcification is an important domain of research and may not replace the established methods in the near future. However, as the experience with this powerful approach becomes substantial, ^{18}F-NaF PET may play a major role in the evaluation of the metabolic activity of calcified brain lesions.

CONCLUSION

On the basis of the scientific data that we have described in this article, ^{18}F-NaF could be used in the assessment of physiologic calcification in several intracranial structures. We report a significant association between ^{18}F-NaF uptake and aging as well as HU in the calcified choroid plexus and epithalamus. Our findings further support the growing interest to use ^{18}F-NaF for detecting extraosseous, molecular calcification and this powerful probe has potential applications in the evaluation of various age-related, neurodegenerative brain calcifications.

DISCLOSURE

This study was funded by the Anna Marie and Christian Rasmussen's Memorial Foundation, University of Southern Denmark, Odense, Denmark, and the Jørgen and Gisela Thrane's Philanthropic Research Foundation, Broager, Denmark. No other potential conflict of interest relevant to this article was reported.

ACKNOWLEDGMENTS

We thank the staff of the CAMONA study and the study participants for their valuable contributions.

REFERENCES

1. Blau M, Nagler W, Bender MA. Fluorine-18: a new isotope for bone scanning. *J Nucl Med.* 1962;3:332–334.
2. Schirrmeister H, Guhlmann A, Kotzerke J, et al. Early detection and accurate description of extent of metastatic bone disease in breast cancer with fluoride ion and positron emission tomography. *J Clin Oncol.* 1999;17:2381–2389.
3. Raynor W, Houshmand S, Gholami S, et al. Evolving role of molecular imaging with ^{18}F-sodium fluoride PET as a biomarker for calcium metabolism. *Curr Osteoporos Rep.* 2016;14:115–125.
4. Adesanya O, Sprowson A, Masters J, Hutchinson C. Review of the role of dynamic ^{18}F-NaF PET in diagnosing and distinguishing between septic and aseptic loosening in hip prosthesis. *J Orthop Surg Res.* 2015;10:5–15.
5. Wilson GH, 3rd, Gore JC, Yankeelov TE, et al. An approach to breast cancer diagnosis via PET imaging of microcalcifications using ^{18}F-NaF. *J Nucl Med.* 2014;55:1138–1143.
6. Wu J, Zhu H, Ji H. Unexpected detection of brain metastases by ^{18}F-NaF PET/CT in a patient with lung cancer. *Clin Nucl Med.* 2013;38:e429–432.
7. Blomberg BA, de Jong PA, Thomassen A, et al. Thoracic aorta calcification but not inflammation is associated with increased cardiovascular disease risk: results of the CAMONA study. *Eur J Nucl Med Mol Imaging.* 2017;44:249–258.
8. Fiz F, Morbelli S, Piccardo A, et al. ^{18}F-NaF uptake by atherosclerotic plaque on PET/CT imaging: inverse correlation between calcification density and mineral metabolic activity. *J Nucl Med.* 2015;56:1019–1023.

9. Derlin T, Toth Z, Papp L, et al. Correlation of inflammation assessed by ^{18}F-FDG PET, active mineral deposition assessed by ^{18}F-fluoride PET, and vascular calcification in atherosclerotic plaque: a dual-tracer PET/CT study. *J Nucl Med.* 2011;52:1020–1027.
10. Asmar A, Simonsen L, Svolgaard B, et al. Unexpected diffuse ^{18}F-NaF uptake in the lung parenchyma in a patient with severe hypercalcemia due to myelomatosis. *Clin Nucl Med.* 2017;42:68–69.
11. Shao F, Zou Y, Cai L, et al. Unexpected detection of urinary bladder cancer on dual phase ^{18}F-NaF PET/CT in a patient with back pain. *Clin Nucl Med.* 2016;41:902–904.
12. Al-Zaghal A, Werner TJ, Høilund-Carlsen PF, Alavi A. The detection of uterine leiomyoma (fibroid) calcifications on ^{18}F-NaF PET/CT. *Clin Nucl Med.* 2018;43: e287–e288.
13. Saboury B, Ziai P, Alavi A. Detection and quantification of molecular calcification by PET/computed tomography: a new paradigm in assessing atherosclerosis. *PET Clin.* 2011;6:409–415.
14. Deng H, Zheng W, Jankovic J. Genetics and molecular biology of brain calcification. *Ageing Res Rev.* 2015;22:20–38.
15. Grech R, Grech S, Mizzi A. Intracranial calcifications: a pictorial review. *Neuroradiol J.* 2012;25:427–451.
16. Blomberg BA, Thomassen A, Takx RAP, et al. Delayed ^{18}F-fluorodeoxyglucose PET/CT imaging improves quantitation of atherosclerotic plaque inflammation: results from the CAMONA study. *J Nucl Cardiol.* 2014;21:588–597.
17. D'Agostino RB Sr, Vasan RS, Pencina MJ, et al. General cardiovascular risk profile for use in primary care: the Framingham Heart Study. *Circulation.* 2008;117: 743–753.
18. Blomberg BA, Thomassen A, de Jong PA, et al. Coronary fluorine-18-sodium fluoride uptake is increased in healthy adults with an unfavorable cardiovascular risk profile: results from the CAMONA study. *Nucl Med Commun.* 2017;38: 1007–1014.
19. Blomberg BA, Thomassen A, Takx RA, et al. Delayed sodium ^{18}F-fluoride PET/CT imaging does not improve quantification of vascular calcification metabolism: results from the CAMONA study. *J Nucl Cardiol.* 2014;21:293–304.
20. Daghighi MH, Rezaei V, Zarrintan S, Pourfathi H. Intracranial physiological calcifications in adults on computed tomography in Tabriz. *Folia Morphol (Warsz).* 2007;66:115–119.
21. Kıroğlu Y, Calli C, Karabulut N, Oncel C. Intracranial calcification on CT. *Diagn Interv Radiol.* 2010;16:263–269.
22. Kendall B, Cavanagh N. Intracranial calcification in paediatric computed tomography. *Neuroradiology.* 1986;28:324–330.
23. Maślińska D, Laure-Kamionowska M, Deregowski K, Maśliński S. Association of mast cells with calcification in the human pineal gland. *Folia Neuropathol.* 2010;48:276–282.
24. Zimmerman RA, Bilaniuk LT. Age-related incidence of pineal calcification detected by computed tomography. *Radiology.* 1982;142:659–662.
25. Beall SS, Pattern BM, Mallette L, Jankovic J. Abnormal systemic metabolism of iron porphyrin, and calcium in Fahr's syndrome. *Ann Neurol.* 1989;26:569–575.
26. Duckett S, Galle P, Escourolle R, Poirier J, Hauw JJ. Presence of zinc aluminum, magnesium in striopalledodentate (SPD) calcifications (Fahr's disease): electron probe study. *Acta Neuropathol (Berl).* 1977;38:7–10.
27. Costeas A, Woodard HQ, Laughlin JS. Depletion of ^{18}F from blood flowing through bone. *J Nucl Med.* 1970;11:43–45.
28. Bastawrous S, Bhargava P, Behnia F, Djang DS, Haseley DR. Newer PET application with an old tracer: role of ^{18}F-NaF skeletal PET/CT in oncologic practice. *Radiographics.* 2014;34:1295–1316.
29. Grant FD, Fahey FH, Packard AB, Davis RT, Alavi A, Treves ST. Skeletal PET with ^{18}F-fluoride: applying new technology to an old tracer. *J Nucl Med.* 2008;49: 68–78.
30. Czernin J, Satyamurthy N, Schiepers C. Molecular mechanisms of bone ^{18}F-NaF deposition. *J Nucl Med.* 2010;51:1826–1829.
31. Blake GM, Park-Holohan SJ, Cook GJ, Fogelman I. Quantitative studies of bone with the use of ^{18}F-fluoride and ^{99m}Tc-methylene diphosphonate. *Semin Nucl Med.* 2001;31:28–49.
32. Kwak R, Takeuchi F, Yamatomo N, Nakamura T, Kadoya S. Intracranial physiological calcification on computed tomography (part 2): calcification in the choroid plexus of the lateral ventricles. *No To Shinkei.* 1988;40:707–711.
33. Whitehead MT, Oh C, Raju A, Choudhri AF. Physiologic pineal region, choroid plexus, and dural calcifications in the first decade of life. *AJNR.* 2015;36: 575–580.
34. Yalcin A, Celyan M, Bayraktutan OF, Sonkaya AR, Yuce I. Age and gender related prevalence of intracranial calcifications in CT imaging; data from 12,000 healthy subjects. *J Chem Neuroanat.* 2016;78:20–24.
35. Tapp E, Huxley M. The histological appearance of the human pineal gland from puberty to old age. *J Pathol.* 1972;108:137–144.
36. Wu YW, Hess CP, Singhal NS, Groden C, Toro C. Idiopathic basal ganglia calcifications: an atypical presentation of PKAN. *Pediatr Neurol.* 2013;49: 351–354.
37. Go JL, Zee CS. Unique CT imaging advantages: hemorrhage and calcification. *Neuroimaging Clin N Am.* 1998;8:541–558.
38. Atlas SW, Grossman RI, Hackney DB, et al. Calcified intracranial lesions: detection with gradient-echo-acquisition rapid MR imaging. *AJR.* 1988;150:1383–1389.
39. Livingston JH, Stivaros S, Van Der Knaap MS, Crow YJ. Recognizable phenotypes associated with intracranial calcification. *Dev Med Child Neurol.* 2013;55: 46–57.
40. Reichenbach JR, Schweser F, Serres B, Deistung A. Quantitative susceptibility mapping: concepts and applications. *Clin Neuroradiol.* 2015;25:225–230.
41. Livingston JH, Stivaros S, Warren D, Crow YJ. Intracranial calcification in childhood: a review of aetiologies and recognizable phenotypes. *Dev Med Child Neurol.* 2014;56:612–626.
42. Lago EG, Baldisserotto M, Hoefel Filho JR, Santiago D, Jungblut R. Agreement between ultrasonography and computed tomography in detecting intracranial calcifications in congenital toxoplasmosis. *Clin Radiol.* 2007;62:1004–1011.